The effect of slatted screens on waves

S. Crowley and R. Porter
School of Mathematics, University of Bristol, Bristol, BS8 1TW,UK
*(*sarah.crowley@bristol.ac.uk, richard.porter@bristol.ac.uk*)*

Abstract. A linearised model is proposed for the transmission of waves through thin vertical porous barriers, where both the inertial and dominant quadratic drag effects are included. A boundary-value problem is developed in which linear boundary conditions holding along the length of the screen are derived from a pair of canonical wave problems, one including an exact geometric description of a slatted screen to determine an inertia coefficient and the other using a quadratic drag law to determine an equivalent linear drag coefficient.

The model is then applied to range of wave scattering and sloshing problems involving thin vertical slatted screens in various settings. In each case results are verified by comparison to the solution of a direct nonlinear calculation where the effects of drag have been isolated. We show that the solution to our canonical problem provides a good approximation to the solution of each of the model problems.

Keywords: water waves, slatted screens, inertial effects, quadratic drag law

1. Introduction

There is a wide range of problems that have been studied involving fluid flow and wave transmission through porous barriers and thin screens. Research has been conducted with application to their use as breakwaters within harbours and as damping devices such as those used in Tuned Liquid Dampers (TLDs).

In the context of porous barriers, Sollitt and Cross (1972) investigated the reflection and transmission of waves through permeable structures of finite width such as rubble mound breakwaters. The authors analysis begins with the unsteady equations of motion for fluid flow within the structure in which the convection term is neglected. Two sources of drag are included, one linear in velocity and associated with viscous effects and the other quadratic in velocity and associated with turbulent drag. These terms are then linearised, using the principle of equivalent work, such that the pressure gradient through the permeable breakwater is given in terms of a linear resistance coefficient and an added mass coefficient of the medium. The former is then determined via an iterative procedure, whilst the latter must be determined experimentally - but in practice is taken to be zero by the authors (and others Madsen (1974), Dalrymple *el al.* (1991), Yu (1995), Isaacson (1998) although Sulisz (1985) shows better correlation

with experimental data when the added mass coefficient is taken to be unity in dimensionless units). Either side of the breakwater linear wave theory is adopted and general solutions in those regions are matched to a solution within the porous breakwater with appropriate continuity of pressure and flux conditions applied across the matching interfaces.

The effect of horizontal porous plates on waves has also been extensively studied using linear water-wave theory. Wu, Wan and Fang (1998) provide a good literature review on the subject, implementing a continuous approximation via a porous effect parameter making the assumption that the material structure of the plate consists of very fine pores and thus the normal velocity of the fluid passing through the plate is linearly proportional to the pressure jump across it - akin to a viscous Darcy type law.

In this paper however, we are concerned with thin slatted vertical screens as opposed to those considered by Sollitt and Cross (1972) of some finite width. Yu (1995) derives a porous boundary condition based on the formulation of Sollitt and Cross (1972) but for the diffraction of waves by thin porous barriers - assuming the length scale of the wave motion within the porous medium to be significantly longer than the thickness of the breakwater, such that the thickness can be neglected. The condition assumes that the jump in pressure is proportional to the velocity of the flow through the barrier, where, rather than determining a linear resistance coefficient via an iterative method, the author simply assumes it to be known. Initially, Yu solves a two dimensional problem in which an incident wave propagates towards a vertical thin porous barrier. Comparison between theory and experimental data gathered by Kondo and Toma (1972) is made, however the data was collected from experiments in which the small thickness assumption does not hold. This solution is then used to provide the outer solution when Yu goes on to investigate the three-dimensional problem of the diffraction of waves by a semi-infinite porous plate via the application of boundary layer theory. Yu (1995) concludes that neglecting the inertial effect of flow through the porous medium underestimates the actual damping effect of a porous breakwater.

McIver (1999) also follows Yu's formulation to obtain a boundary condition at a thin vertical porous breakwater of semi-infinite horizontal extent and shows that this three-dimensional diffraction problem has an explicit solution, found via the Wiener-Hopf technique, valid for arbitrary angle of wave incidence. McIver (2005) later applies the same boundary condition in order to consider the diffraction of an incident wave by discrete sections of thin vertical porous breakwater each of finite length. In both McIver (1999) and McIver (2005), the actual parameters used at the porous breakwaters to simulate the effect

of inertia and damping appear to have little connection to physical quantities.

Evans (1990) considered analytically the possibility of using a series of vertical thin porous screens in narrow wave tanks experiments to dissipate waves and reduce reflections back into the tank. Evans (1990) chose in his work to follow the linear screen conditions derived by Tuck (1975). As in Sollitt and Cross (1972) and Yu (1975) these are again represented by averaged conditions over the vertical extent of the screen in which inertial and drag effects are considered separately before combining through addition. Unlike Sollitt and Cross (1972), Tuck (1975) assumes dominance of viscous dissipation by adopting a Darcy type law for the pressure drop across the screen. Whilst this may be appropriate for slow flow, in general the Reynolds numbers in problems of practical importance being considered here imply viscous effects should be small. Tuck (1975) also provides an expression for the inertia or blockage coefficient at the screen on the basis of long wavelengths compared to the gap/slat structure of the screen using a method based on matched asymptotics.

Continuing with thin porous barriers, Bennett *et al.* (1992) adopt a nonlinear condition based on work by Mei *et al.* (1983) to determine the reflection coefficient from a breakwater with and without a backing wall, the method is validated by comparison to experimental results. Similarly to Yu (1995) and McIver (1999), linearised wave theory is adopted either side of the barrier and matching conditions applied across the barrier which is regarded mathematically as a line. The jump in pressure across the screen is described by a quadratic drag law with a head loss coefficient C_D, and a screen-averaged inertial (or blockage) coefficient L - both empirically determined based on the porosity of the barrier. Mei *et al.* (1983) uses long wavelength analysis to suggest a form for L, which coincides with that given by Tuck (1975).

Baffles and thin porous screens are also installed in tanks in order damp the sloshing motion of the contained fluid. Such tanks have specific application to act as TLDs of which Tait *et al.* (2005), (2008) have researched extensively. Tait *et al.* (2005) develop both a linear and nonlinear numerical model of a TLD with multiple screens. In each case inertial effects are neglected, but an empirically determined pressure-loss coefficient is proposed, following Baines and Peterson (1951) for steady flow, and dependent on the solidity ratio of the screen. Faltinsen *et al.* (2010) utilise the same screen-averaged nonlinear pressure drop condition in deriving a two-dimensional model for liquid sloshing in a rectangular tank with a single centrally-placed slatted screen, again choosing to neglect inertia. Faltinsen and Timokha (2011) go on to consider again the same sloshing problem but this time for a slatted

screen of a prescribed geometry. The authors are concerned with the effect of varying the porosity and the number and position of slots in the screen on the resonant frequencies associated with the tank. They adopt a similar approach to that introduced by Porter & Evans (1995) based on a Galerkin approximation but with a different choice of expansion function which arguably is more complicated to compute. Faltinsen *et al.* (2011) then return to using a nonlinear pressure drop condition, but use the method of Faltinsen and Timokha (2011) to approximate the approach velocity of the flow through the screen.

It is evident that there is no clear consensus on what conditions should be applied at porous barriers and thin screens when considering scattering and sloshing problems. With this in mind, we focus our attention on the propagation of waves through thin vertical porous barriers and the conditions to be applied there.

In order to obtain the mathematical solution to such problems we require a screen-averaged linear relationship between the flux and pressure drop at the screen. This is modelled via a complex coefficient which includes a real part associated with the added inertia (a blockage coefficient) provided by the constrictions in the screen and an imaginary part associated with damping. We take aspects of several of the models reviewed above and develop a model which includes both the inertial and the dominant quadratic drag effects with the aim to model the pair of effects as accurately as possible.

For the inertia coefficient, rather than the analytic description used by Tuck (1975) and Mei *et al.* (1983) based on long wavelength analysis, Section 2.1 outlines a method for relating a screen-averaged coefficient to a calculation based on an exact description of the slatted screen structure. This is shown numerically to tend to the results of Tuck (1975) and Mei *et al.* (1983) as the wavelength to gap width ratio becomes large. In Section 2.2, we derive a screen-averaged equivalent linear drag coefficient from a calculation based on the implementation of a quadratic drag law. In both cases we consider a single canonical problem; the scattering of a normal incident wave by a single thin porous barrier. The purpose of this canonical problem is to act as the basis of an approximation to a variety of more complicated but related problems.

In order to assess the accuracy of this approximation in the problems considered we compare the equivalent linear results using the nonlinear canonical problem with a direct nonlinear calculation of drag effects only. Starting with a simple wavemaker next to a screen, we increase the complexity of the problems studied and culminate in considering the fluid response due to the forced motion of a rectangular tank with a single centrally-placed slatted screen. In most situations, the agreement

is found to be excellent. For the case of waves incident to a single screen when both isolated and in front of an impermeable wall, we make comparisons with experiments and numerical results produced by a Bennett *et al.* (1992). Agreement is again shown to be good.

2. Waves incident on a single slatted screen

Parallel-crested small-amplitude waves propagate on a fluid of constant depth h and are normally-incident on a thin horizontally-slatted screen occupying the plane $x = 0$. The resulting fluid motion takes place in the two-dimensional (x, y) plane and we assume linearised kinematic and dynamic conditions apply on the mean free surface of the fluid, $y = 0$. The fluid is incompressible and, in the bulk of the fluid away from the screen, the flow is assumed to be irrotational. Thus, the fluid is governed in the bulk by a velocity potential $\Phi(x, y, t)$ satisfying

$$\nabla^2\Phi = 0 \tag{2.1}$$

with

$$\Phi_y = 0, \qquad \text{on } y = h, \qquad \text{and} \qquad g\Phi_y + \Phi_{tt} = 0, \qquad \text{on } y = 0, \tag{2.2}$$

g being gravitational acceleration. We require conditions relating properties of the flow on one side of the screen to the other. Formally, we isolate a narrow strip of fluid either side of the slatted screen and examine the effects of the local flow field in the presence of the slatted barrier, before contracting those conditions onto the line occupied by the screen thereby allowing us to formulate approximate boundary conditions on the screen. See Bennett *et al.* (1992) whose work closely follows that of Mei (1983).

Such a process readily results in a condition expressing continuity of horizontal velocity across the screen, or

$$[\Phi_x]_{x=0^-}^{x=0^+} = 0, \qquad 0 < y < h, \tag{2.3}$$

where $[u]$ denotes the jump in u, whilst (2.1) now holds throughout the fluid domain. A dynamic condition is also derived in the form

$$[\Phi_t(x, y, t)]_{x=0^-}^{x=0^+} = \tfrac{1}{2}C_D V(y, t)|V(y, t)| + LV_t(y, t), \qquad 0 < y < h, \tag{2.4}$$

where $V(y, t) \equiv \Phi_x(0, y, t)$ is the horizontal velocity of the fluid relative to that of the screen and C_D and L are empirically determined. Here, C_D represents a drag coefficient for the screen, and L represents an

inertia (or blockage) coefficient accounting for the added inertia felt by the fluid as it accelerates through the constrictions in a slatted screen.

Mei (1983) uses a local analysis of the flow field to suggest forms for C_D and L, the latter also based on a long wavelength analysis equivalent to that used by Tuck (1975).

We take a different approach, and empirically determine the drag and inertia effects from idealised mathematical models, outlined in following two subsections, in which the two effects of inertia and drag are isolated from one another and treated separately. Whilst the condition (2.4) should be regarded as an 'averaged condition' which does not distinguish the local gap/slat structure of the screen, the approximation of an equivalent inertia coefficient L outlined in §2.1 is derived from an exact description of the screen. In contrast, the drag term is approximated through a continuous description of the screen properties, the emphasis in §2.2 being on developing an equivalent linear drag law from a model quadratic drag law calculation.

The aim of such an approach is to derive simple, but realistic, linear relations between the pressure jump and the velocity across a screen having constant properties along its length which can then be used in other settings.

2.1. The screen inertia coefficient

The aim here is to develop an accurate description of the blockage effect of a perforated screen which can be applied uniformly across the entire screen. We follow and extend the approach introduced by Porter & Evans (1995) to consider the scattering of waves by a vertical slatted barrier with multiple gaps.

We consider a two-dimensional wave scattering problem involving a single perforated screen at $x = 0$ in a horizontally-unbounded domain under forcing from an incident wave from $x = -\infty$.

The screen is thin and rigid, and contains N gaps of equal size $2d$, equally-spaced along the screen, occupying $y \in L_j$, $L_j = (y_j^-, y_j^+)$, $j = 1, \ldots, N$, as in figure 1. Specifically, we choose the centre of the gaps to be positioned at $y = c_j = (2j-1)h/2N$ where $y = h$ is the bottom of the fluid, with $d = hp/2N$ and p is the porosity of the screen. Thus, rigid parts of the screen extend through the surface and connect to the fluid bottom, a choice which simplifies the solution process. Of course, other arrangements could be chosen.

With C_D set to zero in (2.4), the governing boundary-value problem for Φ is linear and assuming incident waves of a single radian frequency ω and amplitude A from $x = -\infty$ allows us to write the total potential

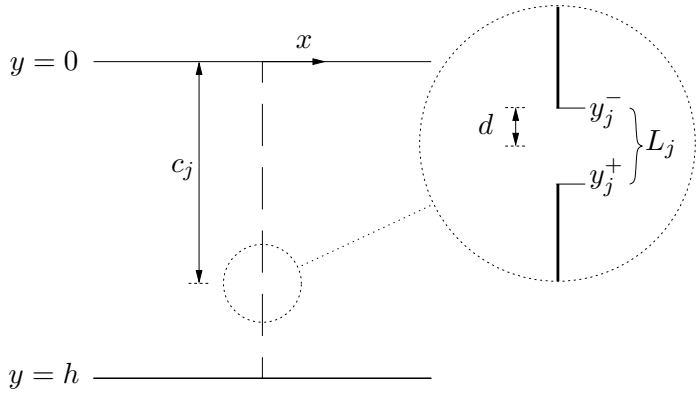

Figure 1. Definition sketch for scattering by a vertical porous screen.

as

$$\Phi(x, y, t) = \Re\left\{\frac{\mathrm{i}gh\hat{A}}{\omega\psi_0(0)}\phi(x, y)\mathrm{e}^{-\mathrm{i}\omega t}\right\} \tag{2.5}$$

where $\hat{A} = A/h$ and ψ_0 is defined below in (2.11). The complex dimensionless potential ϕ now satisfies

$$\nabla^2\phi = 0, \qquad \text{in the fluid} \tag{2.6}$$

with

$$\phi_y = 0, \qquad \text{on } y = h \qquad \text{and} \qquad \phi_y - K\phi = 0, \qquad \text{on } y = 0 \tag{2.7}$$

where $K = \omega^2/g$. Additionally,

$$[\phi_x]_{x=0^-}^{x=0^+} = 0, \qquad 0 < y < h, \tag{2.8}$$

with

$$\phi_x = 0, \qquad \text{for } y \in L_b \qquad \text{and} \qquad [\phi]_{x=0^-}^{x=0^+}, \qquad \text{for } y \in L_g. \tag{2.9}$$

where $L_g = \cup_{j=1}^{N} L_j$ is the union of the gaps and $L_b = (0, h)\backslash L_g$ is the union of the slats.

The conditions (2.9) satisfy the exact conditions on the screen and the solution of (2.6)–(2.9) will be connected to a screen-averaged condition towards the end of this section.

The solution is based on expanding in depth eigenfunctions, defined as

$$\psi_n(y) = N_n^{-1/2}\cos k_n(h - y), \qquad N_n = \frac{1}{2}\left(1 + \frac{\sin 2k_n h}{2k_n h}\right) \tag{2.10}$$

for $n = 0, 1, 2, \ldots$ where k_n $(n \geq 1)$ are the real positive roots of $K = -k_n \tan k_n h$ whilst $k_0 = -\mathrm{i}k$ where k is the real positive root of $K = k \tanh kh$ so that

$$\psi_0(y) = N_0^{-1/2} \cosh k(h-y), \qquad N_0 = \frac{1}{2}\left(1 + \frac{\sinh 2kh}{2kh}\right) \tag{2.11}$$

The eigenfunctions in (2.10) are normalised so that

$$\frac{1}{h}\int_0^h \psi_n(y)\psi_m(y)\mathrm{d}y = \delta_{mn}, \qquad m, n = 0, 1, \ldots \tag{2.12}$$

where δ_{mn} is the Kronecker delta.

We can now write separation solutions in $x < 0$ and $x > 0$ as

$$\phi(x,y) = (\mathrm{e}^{\mathrm{i}kx} + R\mathrm{e}^{-\mathrm{i}kx})\psi_0(y) - \sum_{n=1}^{\infty} a_n \mathrm{e}^{k_n x}\psi_n(y), \tag{2.13}$$

and

$$\phi(x,y) = T\mathrm{e}^{\mathrm{i}kx}\psi_0(y) + \sum_{n=1}^{\infty} a_n \mathrm{e}^{-k_n x}\psi_n(y), \tag{2.14}$$

where the expansion coefficients a_n are the same in $x < 0$ and $x > 0$ such that (2.8) is satisfied provided $R + T = 1$ where R, T are the reflection and transmission coefficients.

Letting $U(y) = \phi_x(0, y)$ and using (2.12) allows us to express all unknowns in (2.13) and (2.14) in terms of $U(y)$ as

$$a_n = -\frac{1}{k_n h}\int_{L_g} U(y)\psi_n(y)\mathrm{d}y, \qquad n \geq 1, \tag{2.15}$$

and

$$\mathrm{i}kh(1-R) = \int_{L_g} U(y)\psi_0(y)\mathrm{d}y, \tag{2.16}$$

since $U(y) = 0$ on any rigid part of the screen. Applying the remaining condition of continuity of fluid pressure across each of the gaps, expressed as $[\phi]^+_- = 0$ for $y \in L_g$, gives

$$\int_{L_g} U(t)K(y,t)\mathrm{d}t = -R\psi_0(y), \qquad y \in L_g, \tag{2.17}$$

after use of (2.15) where

$$K(y,t) = \sum_{r=1}^{\infty} \frac{\psi_r(y)\psi_r(t)}{k_r h}, \tag{2.18}$$

is a weakly singular kernel. The integral operator in (2.18) is real and symmetric (hence self-adjoint) and positive in the space $L_2(L_g)$. A re-scaling $U(y) = -Ru(y)$ eliminates the unknown from (2.17), replacing this equation with

$$\int_{L_g} u(t)K(y,t)\mathrm{d}t = \psi_0(y), \qquad y \in L_g, \tag{2.19}$$

whilst the re-scaling, used in (2.16), allows us to write

$$R = (1 + \mathrm{i}A_u/(kh))^{-1} \qquad \text{where } A_u = \int_{L_g} u(y)\psi_0(y)\mathrm{d}y. \tag{2.20}$$

The solution $u(t)$ to (2.19) is used to determine R through (2.20). This is done by application of the Galerkin variational method in which we write $u(y) \equiv u_i(y)$ for $y \in L_i$, $i = 1, \ldots, N$,

$$u_i(y) \approx \sum_{p=0}^{P} \alpha_p^{(i)} v_p(y - c_i), \tag{2.21}$$

where $\alpha_p^{(i)}$ are expansion coefficients to be determined and v_p are defined as

$$v_p(y) = \frac{T_p(y/d)}{\pi(d^2 - y^2)^{1/2}}, \tag{2.22}$$

(see, for example, Porter & Evans (1995)) in terms of Tchebychev polynomials $T_p(\cdot)$. The form chosen for (2.22) incorporates the anticipated inverse square root singularities in $u_i(y)$ (a function proportional to the fluid velocity) at each of the sharp edges of the perforated screen and that the bounded function $(d^2 - (y - c_i)^2)^{1/2}u_i(y)$ has been expanded in a complete orthogonal set of functions.

Faltinsen and Timokha (2011) used expansions of the form given in (2.21) but with a different choice of expansion function to (2.22) that also includes the square-root behaviour at the end points. The resulting coefficients here (see (2.25) and (2.26)) are arguably easier to compute.

Substitution of (2.22) into (2.21), multiplication through by $v_q(y - c_j)$ for $q = 0, \ldots, P$, $j = 1, \ldots, N$, and integration over $y \in L_j$ is a process which characterises the Galerkin variational method and gives rise to a linear system of algebraic equations for the unknown expansion coefficients written as

$$\sum_{i=1}^{N} \sum_{p=0}^{P} \alpha_p^{(i)} K_{pq}^{(i,j)} = F_{q0}^{(j)}, \tag{2.23}$$

for $q = 0, \ldots, P$, $j = 1, \ldots, N$, where

$$K_{pq}^{(i,j)} = \sum_{r=1}^{\infty} \frac{F_{pr}^{(i)} F_{qr}^{(j)}}{k_r h}, \tag{2.24}$$

and

$$F_{pr}^{(i)} = \int_{L_i} v_p(y - c_i)\psi_r(y)\mathrm{d}y = N_r^{-1/2} \cos\left(k_r(h - c_i) - \tfrac{1}{2}\pi p\right) J_p(k_r d), \tag{2.25}$$

for $r \geq 1$ and with

$$F_{p0}^{(i)} = \begin{cases} N_0^{-1/2} \cosh\left(k(h - c_i)\right) I_p(kd), & p \text{ even}, \\ -N_0^{-1/2} \sinh\left(k(h - c_i)\right) I_p(kd), & p \text{ odd}, \end{cases} \tag{2.26}$$

(for a detailed account of these calculations, see Porter & Evans (1995)) where $J_p(\cdot)$ and $I_p(\cdot)$ are Bessel functions. Typically, numerical results are accurate to 4 decimal places with $P = 2$, and for a truncation of the infinite series in (2.24) at 2000 terms (though the convergence of the series can be accelerated as described in Porter & Evans (1995)). Finally, R is found from (2.20) with the numerical approximation giving

$$A_u \approx \sum_{i=1}^{N} \sum_{p=0}^{P} \alpha_p^{(i)} F_{p0}^{(i)}. \tag{2.27}$$

In contrast to the exact analysis above for a perforated screen with N discretely-defined gaps and an overall porosity of p, we assume a porous screen with constant properties along its vertical extent. Then the expansions for the potential left and right of $x = 0$ are still given by (2.13), (2.14) satisfying (2.8) with $R + T = 1$ but we now pose a condition across the screen of

$$[\phi]_{x=0^-}^{x=0^+} = \frac{\mathbb{C}}{k}\phi_x(0, y), \qquad 0 < y < h, \tag{2.28}$$

which is equivalent to (2.4) with $C_D = 0$ and with (2.5) used, replacing L by $\mathbb{C}/k$. The aim is to find the real dimensionless coefficient $\mathbb{C}$ that best models the exact results. Tuck (1975) used a long-wavelength theory based on matched asymptotics (also repeated in Mei (1983, p.121)) to estimate $\mathbb{C}$ by

$$\mathbb{C} = -\frac{4kd}{\pi p} \log\left(\sin\frac{\pi p}{2}\right), \tag{2.29}$$

where p is the porosity of the screen. Using (2.13), (2.14) and applying (2.28), assuming that $\mathbb{C}$ is given, readily yields reflection and

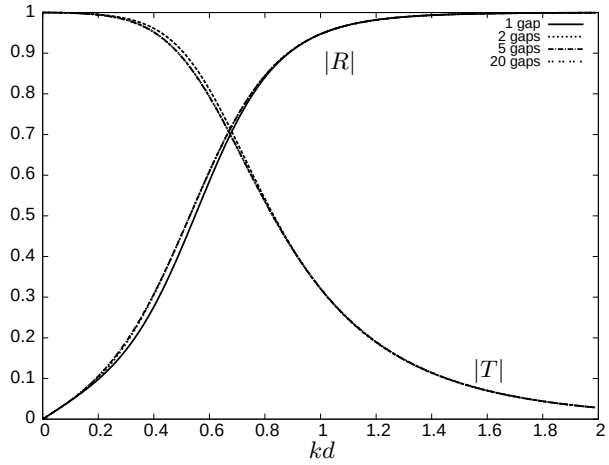

Figure 2. $|R|$ and $|T|$ for a screen of porosity $p = 0.5$ with an increasing number of gaps.

transmission coefficients

$$R = \frac{\mathbb{C}}{\mathbb{C} + 2\mathrm{i}} \qquad \text{and} \qquad T = \frac{2\mathrm{i}}{\mathbb{C} + 2\mathrm{i}}, \tag{2.30}$$

in terms of $\mathbb{C}$. Alternatively, if R and T are known then the value of $\mathbb{C}$ is defined by

$$\mathbb{C} = \frac{2\mathrm{i}R}{T}, \tag{2.31}$$

which is readily shown to be real. Hence, with the exact R and T computed from the first part of this section for a screen with N discrete gaps along its length (2.31) defines a $\mathbb{C}$ for a screen with continuous properties assumed along its length which gives exactly the same values of R and T.

In figure 2 we show results for $|R|$ and $|T|$ against kd for $N = 1, 2, 5, 20$ gaps in a screen with constant porosity of $p = 0.5$. It is seen that curves of reflection and transmission converge rapidly as N increases, and we are able to infer accurate approximations to R and T for a porous screen and hence $\mathbb{C}$ from (2.31) from results with $N = 5$. Figure 3(a) shows the variation of $|R|$ with kd for different values of porosity, p. The reflected amplitude increases monotonically from zero as the wavelength decreases and does so more rapidly for less porous screens. Shown in figure 3(b) are curves of $|R|$ and $|T|$ given by the Tuck (1975) and Mei (1983) relation (2.28) with (2.29). As expected, Tuck's model only agrees with our computed results when $kd \ll 1$.

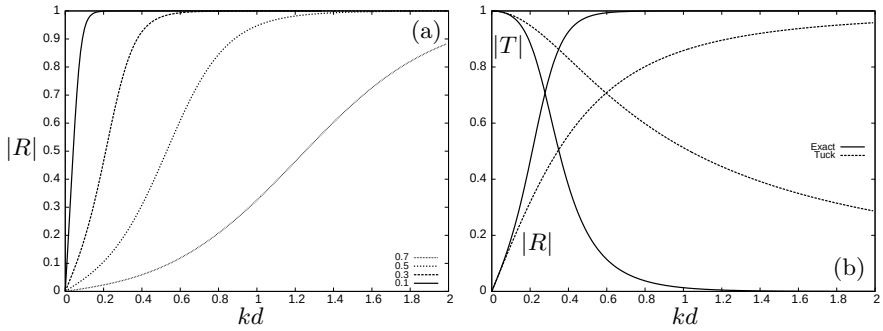

Figure 3. In panel (a): $|R|$ for a screen with 5 gaps of varying porosity, $p = 0.7, 0.5, 0.3$ and 0.1. In panel (b): $|R|$ and $|T|$ for a screen of porosity $p = 0.3$, compared with Tuck's (1975) long wavelength results.

2.2. Estimating the screen drag coefficient

In this section we isolate the effects of drag by setting $L = 0$ in (2.4). It is not obvious how to determine a screen-averaged drag coefficient from an exact description of the screen, thus in contrast to the previous section here the aim is to determine a linear screen-averaged drag coefficient from a calculation based on a quadratic drag law based on empirical experimental results for the quadratic drag coefficient C_D in terms of the porosity, p (see later). There are some similarities in our approach to Mei (1983) and Bennett *et al.* (1992).

With $L = 0$, (2.4) expresses the condition for pressure drop across the screen and is written in terms of the usual turbulent drag law

$$[P(x, y, t)]_{x=0^-}^{x=0^+} = -\tfrac{1}{2}\rho C_D V(y, t)|V(y, t)|, \qquad 0 < y < h, \qquad (2.32)$$

where $P = -\rho\Phi_t$ is the dynamic pressure and $V = \Phi_x(0, y, t)$. The quadratic velocity dependence in the boundary condition implies that an incident wave of a single radian frequency ω introduces a multi-frequency response. Thus expanding Φ in a Fourier time-series in multiples of ω and retaining just the fundamental frequency response (the Fourier coefficient of first term is $8/3\pi$ whilst the next term at frequency 3ω is much smaller than ω and justifies this assumption) transforms (2.32), using (2.5), into the condition

$$[\phi(x, y)]_{x=0^-}^{x=0^+} = \mathrm{i}\frac{\mathbb{K}_{NL}}{k^2}\phi_x(0, y)|\phi_x(0, y)|, \qquad 0 < y < h, \qquad (2.33)$$

where $\phi(x,y)$ is the complex potential associated with the time variation $\mathrm{e}^{-\mathrm{i}\omega t}$ and

$$\mathbb{K}_{NL} = \frac{4C_D k^2 gh|\hat{A}|}{3\pi\omega^2\psi_0(0)} \equiv \frac{4C_D N_0^{1/2} kh|\hat{A}|}{3\pi \sinh kh} \tag{2.34}$$

is a dimensionless proxy for the drag coefficient, C_D. In the above, $K = \omega^2/(gk) = \tanh kh$ has been used and N_0 is given in (2.11).

The problem now to be solved for ϕ includes the non-linear condition (2.33) at the screen alongside the usual linear conditions (2.6)–(2.8).

For a wave incident from $x = -\infty$ on the screen, we could reuse the expansions for ϕ given in (2.13), (2.14) already satisfying (2.6)–(2.8) provided $R + T = 1$ when it remains only to apply (2.33). In view of later developments in the paper however, we choose to take a more general scattering problem in which waves of amplitudes A and AB (A and B both given) are incident from $x = -\infty$ and $x = +\infty$ respectively. Then expansions in $x < 0$ and $x > 0$, satisfying (2.6)–(2.8) are given by

$$\phi = (\mathrm{e}^{\mathrm{i}kx} + R^-\mathrm{e}^{-\mathrm{i}kx})\psi_0(y) - \sum_{n=1}^{\infty} a_n \mathrm{e}^{k_n x}\psi_n(y) \tag{2.35}$$

and

$$\phi = (B\mathrm{e}^{-\mathrm{i}kx} + R^+\mathrm{e}^{\mathrm{i}kx})\psi_0(y) + \sum_{n=1}^{\infty} a_n \mathrm{e}^{k_n x}\psi_n(y) \tag{2.36}$$

respectively, where the amplitude of the incident wave has been nondimensionalised to unity and (2.8) requires that $1 + B = R^- + R^+$ and $R^\pm$ are the outgoing wave amplitudes to $\pm\infty$. It helps to introduce a coefficient a_0 defined such that $a_0 = 1 - R^-$. It follows that

$$\phi_x(0,y) = -\sum_{n=0}^{\infty} k_n a_n \psi_n(y), \tag{2.37}$$

and

$$[\phi]_{x=0^-}^{x=0^+} = (2B-2)\phi_0(y) + 2\sum_{n=0}^{\infty} a_n\psi_n(y) \tag{2.38}$$

Applying the non-linear screen condition (2.33), multiplying by $\psi_m(y)$ and integrating over $0 < y < h$ gives the infinite system of complex non-linear equations

$$(2-2B)\delta_{m0} - 2a_m = \mathrm{i}\mathbb{K}_{NL}\sum_{n=0}^{\infty}\frac{k_n a_n}{kh}\int_0^h \left|\sum_{r=0}^{\infty}\frac{k_r a_r \psi_r(y)}{k}\right| \psi_n(y)\psi_m(y)\mathrm{d}y, \tag{2.39}$$

for $m = 0, 1, \ldots$. Numerically, this system is truncated to a system of $M+1$ equations, which determine a_m for for $m = 0, 1, \ldots, M$. Typically $M = 10$ is sufficient for convergence of a_0 to a number of decimal places. We note that when $\mathbb{K}_{NL} = 0$, the explicit solution is $a_m = (1 - B)\delta_{m0}$. We use this to solve the non-linear equations by numerically replacing $\mathbb{K}_{NL}$ by the factor $\beta\mathbb{K}_{NL}$ in which β is numerically increased from zero to unity, as a means of introducing non-linearity. We find roots by implementing the Newton-Raphson method at each increment of β, computing the integral in (2.39) via a NAG library routine. Once the solution to (2.39) has been determined numerically, then $R^- = 1 - a_0$ and $R^+ = B + a_0$ defines outgoing reflected wave amplitudes and

$$P_{loss} = 1 + |B|^2 - |R^-|^2 - |R^+|^2, \tag{2.40}$$

represents the flux of energy (power) dissipated by the screen, as a proportion of the incoming wave energy.

We note the special case when waves are incident from $x = -\infty$ only and then $B = 0$ and $R^{\pm}$ represent reflection and transmission coefficients denoted by $R = R^-$ and $T = R^+$.

An equivalent screen-averaged linear drag law assumes that (2.33) is replaced by

$$[\phi]_{x=0^-}^{x=0^+} = \mathrm{i}\frac{\mathbb{K}_L}{k}\phi_x(0, y), \qquad 0 < y < h, \tag{2.41}$$

and applying this to the general expansions (2.35) and (2.36) which yield (2.38) results in

$$R^- = \frac{\mathbb{K}_L + 2B}{2 + \mathbb{K}_L} \qquad \text{and} \qquad R^+ = \frac{2 + B\mathbb{K}_L}{2 + \mathbb{K}_L}. \tag{2.42}$$

Alternatively, if $R^{\pm}$ are known then $\mathbb{K}_L$ may be defined by

$$\mathbb{K}_L = \frac{2(R^- - B)}{(1 - R^-)}. \tag{2.43}$$

Hence, to determine an equivalent linear drag coefficient $\mathbb{K}_L$ from a non-linear drag law, we simply use the values of $R^{\pm}$ computed from the non-linear calculation (2.39) in (2.43). When $B = 0$, the reflection and transmission coefficients are $R = R^-$ and $T = R^+ = 1 - R^-$ whilst $\mathbb{K}_L = 2R/T$.

A crude, but simple, approximate linear drag law can derived by estimating the size of $|\phi_x(0, y)|$ in (2.33) to reduce (2.33) to (2.41). Thus, assuming that there is near total transmission at the screen so that $a_m \approx (1 - B)\delta_{m0}$ and estimating $\phi_x(0, y)$, by its average over the

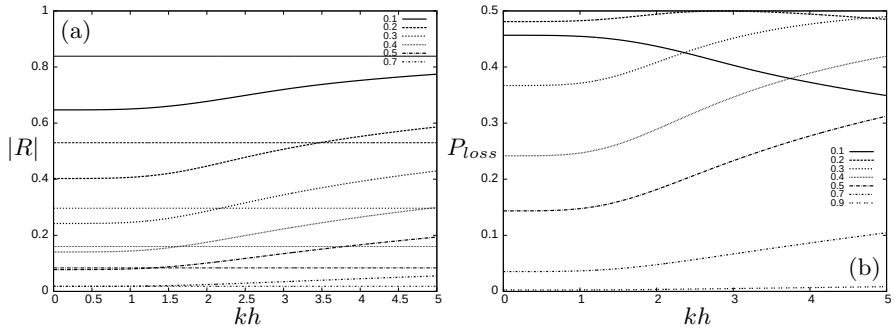

Figure 4. Results of the application of a quadratic drag law at a screen: (a) $|R|$ (the thinner horizontal lines are the long wavelength/low porosity linear approximation given by (2.45)); and (b) P_{loss} for a screen of varying porosity, p and fixed wave amplitude $|\hat{A}| = 0.1$.

vertical extent of the screen implies

$$\frac{|\phi_x|}{k} \approx |(1-B)\psi_0(y)| \approx \frac{|1-B|}{h}\int_0^h \psi_0(y)\mathrm{d}y = N_0^{-1/2}|1-B|\frac{\sinh kh}{kh}, \tag{2.44}$$

and so

$$\mathbb{K}_L \approx N_0^{-1/2}|1-B|\frac{\sinh kh}{kh}\mathbb{K}_{NL} = \frac{4C_D|1-B||\hat{A}|}{3\pi}. \tag{2.45}$$

We might expect this approximation to work well for high porosity and long wavelengths when there is little reflection, but not so well at higher frequencies or for smaller porosity.

Finally, we require an expression for the pressure loss coefficient C_D in terms of p, the porosity. Both Tait (2005) and Mei (1983) write

$$C_D = \left(\frac{1}{pC_c} - 1\right)^2, \tag{2.46}$$

where, according to Tait (2005), empirical evidence suggests that,

$$C_c = 0.405\mathrm{e}^{\pi(p-1)} + 0.595, \tag{2.47}$$

whilst Mei (1983) suggests that C_c can be represented by

$$C_c = 0.4p^3 + 0.6. \tag{2.48}$$

In fact, as can be seen, the two representations are very similar and match well when plotted as a function of p.

In figure 4(a) we plot the variation of $|R|$ with kh for different values of porosity, calculated from (2.35) using the quadratic drag law. In these figures, we imposed a fixed incident wave amplitude of $|\hat{A}| \equiv |A|/h = 0.1$ and $B = 0$ and used (2.48) to determine C_D. Also plotted in figure 4 are the reflected wave amplitudes using (2.42) with the approximate linear drag coefficient in (2.45). As previously anticipated, the linear approximation is good for small kh and high porosity and works less well away from this regime. Considering figure 10(b) of Bennett *et al.* (1992) we see that the theoretical results presented for screens of varying porosity are comparable to ours, with the effects of drag isolated, as shown in figure 4(a). Note that Bennett *et al.* (1992) measure the incident wave height from peak to trough as opposed to the incident wave amplitude measured as the distance from the mean free surface as in this paper. In figure 4(b) we plot the associated fraction of energy, P_{loss}, defined by (2.40) lost at the screen which we observe is bounded by 1/2. This confirms the well-known result from wave energy absorption that no more than half the available power in the incident wave can be absorbed by a wave energy converter with left-right symmetry (see Evans (1976), Mei (1975), Newman (1976)). The general trends seen are that a higher porosity implies less power loss and that as the wavelength shortens, more power is lost although these are rules are not observed across all parameter values.

2.3. Combining coefficients

In the previous two subsections we have presented methods for determining linear screen-averaged conditions when inertia and drag effects are isolated. According to (2.4) where these two effects are added together, we suggest a linear condition replacing (2.4) to be the sum of the two linearised screen-averaged effects of drag and inertia, namely

$$[\phi(x,y)]_{x=0^-}^{x=0^+} = \frac{\gamma}{k}\phi_x(0,y) \qquad \text{where } \gamma = \mathbb{C} + \mathrm{i}\mathbb{K}_L, \tag{2.49}$$

whose components are determined according to the prescription given in §2.1 and §2.2. A condition involving a complex coefficient has been used previously in the context of porous barriers, such as Tuck (1975), Yu (1995) and Isaacson *et al.* (1998).

For a wave of amplitude A from $x = -\infty$ (i.e. $B = 0$ in §2.2) the reflection and transmission coefficients are easily found by using the general expansions (2.35) and (2.36) and applying (2.49) from which we derive reflection and transmission coefficients

$$R = \frac{\gamma}{\gamma + 2\mathrm{i}} \qquad \text{and} \qquad T = \frac{2\mathrm{i}}{\gamma + 2\mathrm{i}}, \tag{2.50}$$

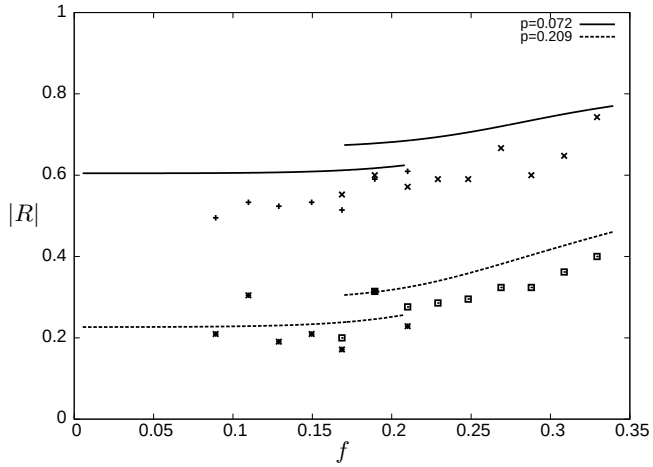

Figure 5. $|R|$ for a screen of porosity $p = 0.072$ and $p = 0.209$ against frequency in Hz. compared with experimental results from Bennett *et al.* (1992). The experiments were performed for two wave spectra producing two sets of results for incident waves of amplitude $\hat{A} = 0.0372$ and $\hat{A} = 0.0581$ covering frequencies relating to wave periods of $4.5 - 14\,\mathrm{s}$ and $2.9 - 6.2\,\mathrm{s}$ respectively.

which is in agreement with (2.30) and (2.42) if either drag or inertia effect is switched off.

Having solved each of the preceding problems of §2.1 and §2.2 individually, the blockage coefficient $\mathbb{C}$ is then determined via (2.31) and $\mathbb{K}_L$ via (2.43). Combining these coefficients as prescribed by (2.49), we evaluate the reflection and transmission coefficients $|R|$ and $|T|$ of an incident wave acting on a single thin vertical porous barrier using (2.50).

In figure 5 we compare the results of our proposed model, including the effects of both drag and inertia at the screen, with experimental results from Bennett *et al.* (1992). The reflection from the screen seems to be mostly overestimated by our model, however this discrepancy may be due to the empirical formula (2.48) used to determine the discharge coefficient C_c. Bennett *et al.* (1992) plot theoretical results obtained with the two limiting values of this formula, $C_c = 0.6$ and $C_c = 1$. Most of the experimental results fall within this range, suggesting that an improved empirical formula should still produce theoretical results within these bounds.

3. Using the single-screen solution to approximate the solution in other settings

In this section we present a variety of problems involving slatted screens in other settings, the purpose in each case to show that the solution of §2 can be used to approximate the solution in each example.

3.1. A wavemaker next to a fixed slatted screen

We consider a fluid of depth h with a fixed slatted screen at $x = 0$. The fluid is unbounded in the positive x direction, and bounded by a vertical impermeable wall oscillating sinusoidally with radian frequency ω and amplitude $\epsilon \ll a$ about a mean position of $x = -a$. The wall acts as a piston wavemaker and the waves created are partly transmitted through the screen at $x = 0$. The governing equations are thus (2.1)–(2.4) supplemented by a linearised kinematic condition

$$\Phi_x = \omega\epsilon\cos\omega t, \qquad \text{on } x = -a. \tag{3.1}$$

We follow earlier arguments to make the single frequency decomposition of the potential

$$\Phi(x, y, t) = \Re\left\{\omega\epsilon\phi(x, y)\mathrm{e}^{-\mathrm{i}\omega t}\right\}, \tag{3.2}$$

such that (3.1) is satisfied by

$$\phi_x(-a, y) = 1 \equiv \sum_{n=0}^{\infty} L_n\psi_n(y), \tag{3.3}$$

where

$$L_n = \frac{1}{h}\int_0^h \psi_n(y)\mathrm{d}y = N_n^{-1/2}\frac{\sin k_n h}{k_n h}, \tag{3.4}$$

after decomposing the forcing into depth eigenfunctions, whilst the usual conditions (2.6)–(2.8) apply to ϕ in addition. We shall consider the application of a screen-averaged flow condition later but first set out a general solution.

In the region $-a < x < 0$ we write

$$\begin{aligned}\phi(x, y) =& \frac{1}{\mathrm{i}k}\left(a_0\mathrm{e}^{\mathrm{i}k(x+a)} - b_0\mathrm{e}^{-\mathrm{i}kx}\right)\psi_0(y)\\ &- \sum_{n=1}^{\infty}\frac{1}{k_n}\left(a_n\mathrm{e}^{-k_n(x+a)} - b_n\mathrm{e}^{k_n x}\right)\psi_n(y),\end{aligned} \tag{3.5}$$

and in $x > 0$ we write

$$\phi(x, y) = \frac{c_0}{\mathrm{i}k}\mathrm{e}^{\mathrm{i}kx}\psi_0(y) - \sum_{n=1}^{\infty}\frac{c_n}{k_n}\mathrm{e}^{-k_n x}\psi_n(y). \tag{3.6}$$

The isolated terms in the pair of equations above will hereafter be subsumed into summations starting at $n = 0$ using the definition $k_0 = -\mathrm{i}k$; they are left exposed in (3.5) and (3.6) to allow the reader to identify $n = 0$ terms as propagating waves. Then, applying (3.3) to (3.5) and a subsequent application of the screen flux continuity condition (2.8) to (3.5) and (3.6) gives the relations between the coefficients of

$$a_n = L_n - b_n \mathrm{e}^{-k_n a} \qquad \text{and} \qquad b_n = \frac{c_n - L_n \mathrm{e}^{-k_n a}}{1 - \mathrm{e}^{-2k_n a}}, \quad n \geq 0. \tag{3.7}$$

Using these relations in (3.5) and (3.6) gives

$$[\phi]_{x=0^-}^{x=0^+} = -2 \sum_{n=0}^{\infty} \frac{(c_n - L_n \mathrm{e}^{-k_n a})}{k_n (1 - \mathrm{e}^{-2k_n a})} \psi_n(y), \tag{3.8}$$

and

$$\phi_x(0, y) = \sum_{n=0}^{\infty} c_n \psi_n(y). \tag{3.9}$$

Posing a linearised screen-averaged condition

$$[\phi(x, y)]_{x=0^-}^{x=0^+} = \frac{\gamma}{k} \phi_x(0, y), \qquad 0 < y < h, \tag{3.10}$$

as in (2.49) where $\gamma = \mathbb{C} + \mathrm{i}\mathbb{K}_L$ then it follows that

$$\frac{c_0 - L_0 \mathrm{e}^{\mathrm{i}ka}}{1 - \mathrm{e}^{2\mathrm{i}ka}} = -\mu_0 c_0, \tag{3.11}$$

where $\mu_0 = -\mathrm{i}\gamma/2$ so that

$$c_0 = \frac{L_0 \mathrm{e}^{\mathrm{i}ka}}{(1 + \mu_0 (1 - \mathrm{e}^{2\mathrm{i}ka}))}, \tag{3.12}$$

is the far-field radiated wave coefficient. It remains to decide on how to map the values of the components of γ from the canonical problems of §2. The value of $\mathbb{C}$ is straightforward and defined by (2.31) which depends implicitly on the porosity p and the number of slats N which defines kd. Of course, its value is approximate, since the problem defining the inertia coefficient $\mathbb{C}$ is different to the one being solved here, but it does not rely upon any extra information about the wave field. The value of $\mathbb{K}_L$ to be used is more complicated because of the inherent non-linearity of the problem from which it is derived. First, we have to map the amplitude of the wavemaker into the amplitude of surface waves incident on the screen. We note that the free surface elevation

$\zeta(x,t)$ is defined by the Bernoulli condition $g\zeta = -\Phi_t$ and assuming $\zeta(x,t) = \Re\{\eta(x)\mathrm{e}^{-\mathrm{i}\omega t}\}$ and using (3.2) we have

$$\eta(x) = -\mathrm{i}K\epsilon\phi(x,0). \tag{3.13}$$

In this problem only propagating waves are incident on the slatted screen from $x < 0$ and the free surface elevation, associated with those incident waves from (3.5) is

$$\eta_{inc}(x) = -\mathrm{i}K\epsilon\frac{\psi_0(0)}{\mathrm{i}k}a_0\mathrm{e}^{\mathrm{i}ka}\mathrm{e}^{\mathrm{i}kx}. \tag{3.14}$$

In other words, the non-dimensional amplitude of the incident wave on the screen in this wavemaker problem is

$$|\hat{A}| = \left|-\frac{K\epsilon\psi_0(0)\mathrm{e}^{\mathrm{i}ka}a_0}{kh}\right| = N_0^{-1/2}\hat{\epsilon}\sinh kh|a_0| \tag{3.15}$$

where $\hat{\epsilon} = \epsilon/h$ is a nondimensional wavemaker amplitude. For a given value of $\hat{\epsilon}$ and $|a_0|$, (3.15) defines the amplitude of a wave incident on the screen. Hence, for a given screen porosity, p, we can use the process outlined in §2.2 with $B = 0$ to define an equivalent linear drag coefficient $\mathbb{K}_L$ to be used to determine the far-field waves via (3.12). However, since $\mathbb{K}_L$ is implicitly a function of $|a_0|$, the solution must be arrived at by numerical iteration using the value of a_0 resulting from the solution

$$a_0 = \frac{L_0(1+\mu_0)}{(1+\mu_0(1-\mathrm{e}^{2\mathrm{i}ka}))} \tag{3.16}$$

which is found from using (3.12) in (3.7). The added complexity of iterating the solution is simply an expected by-product of including non-linearity in the screen condition.

A different approach, and one which we will use to determine the accuracy of the procedure outlined above, is to determine the drag induced by the screen directly. That is, we assume only drag effects hold and using (3.2) in (2.4) with $L = 0$ we see that the non-linear condition at the screen can be written

$$[\phi]_{x=0^-}^{x=0^+} = \mathrm{i}\frac{\mathbb{K}_{NL}}{k^2}\phi_x(0,y)|\phi_x(0,y)| \tag{3.17}$$

where now $\mathbb{K}_{NL} = (4/3\pi)C_D(\omega\epsilon)k^2 = 4C_Dkh\hat{\epsilon}/(3\pi)$ is a proxy for the non-linear drag coefficient in terms of the wavemaker amplitude. Applying (3.17) to (3.8) gives rise to a non-linear system of equations

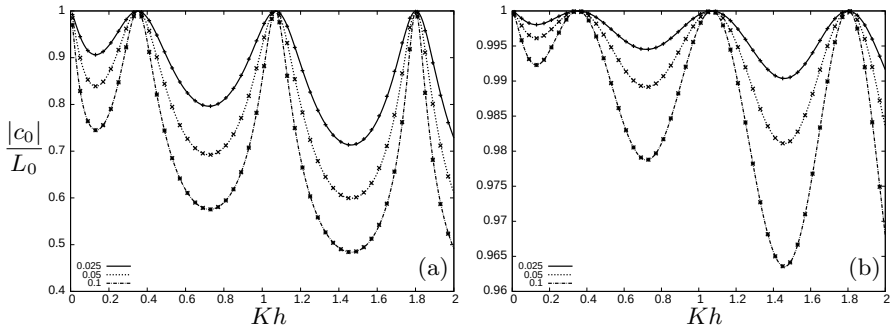

Figure 6. The damping effect $|c_0|/L_0$ for a wavemaker next to a fixed screen with $\frac{a}{h} = 5$ for $\frac{\epsilon}{h} = 0.025, 0.05$ and 0.1. In panel (a): For a screen of porosity $p = 0.25$; (b): $p = 0.75$. Dashed lines show the fully non-linear results and the crosses the equivalent linear results.

similar to those in (2.39), and given by

$$-2\frac{(c_m - L_m \mathrm{e}^{-k_m a})}{k_m h(1 - \mathrm{e}^{-2k_m a})} = \mathrm{i}\mathbb{K}_{NL} \sum_{n=0}^{\infty} \frac{c_n}{h} \int_0^h \left| \sum_{r=0}^{\infty} c_r \psi_r(y) \right| \psi_n(y)\psi_m(y)\mathrm{d}y \qquad (3.18)$$

for $m = 0, 1, \ldots$. As in §2.2 truncating this numerically to a small number (10) of terms is sufficient for the convergence we require and non-linearity can be introduced by a scaling factor on the right-hand side which increases from zero, where the solution $c_m = L_m \mathrm{e}^{-k_m a}$ is explicit, to unity. Once the solution to (3.18) is found numerically, we use various measures to assess the accuracy of the linearised solution via comparison to the solution of the nonlinear problem.

We first consider the power lost through damping over a cycle at the screen at $x = 0$. This given by,

$$W_{out} = -\tfrac{1}{2}\Re\left\{ \mathrm{i}\omega\rho \int_0^h [\phi]_-^+ \bar{\phi}_x \mathrm{d}y \right\}, \qquad (3.19)$$

where the bar represents complex conjugation and $[\phi]_-^+ = \phi(0^+, y) - \phi(0^-, y)$. Applying Green's identity to the potential ϕ and its conjugate $\bar{\phi}$ in both regions $x > 0$ and $x < 0$,

$$\iint_V \bar{\phi}\nabla^2\phi - \phi\nabla^2\bar{\phi}\mathrm{d}x\mathrm{d}y = \int_S \bar{\phi}\frac{\partial\phi}{\partial n} - \phi\frac{\partial\bar{\phi}}{\partial n}\mathrm{d}S, \qquad (3.20)$$

where $\partial/\partial n$ is the derivative of the outward normal to the surface S bounding the volume V. The left-hand side of (3.20) is clearly zero.

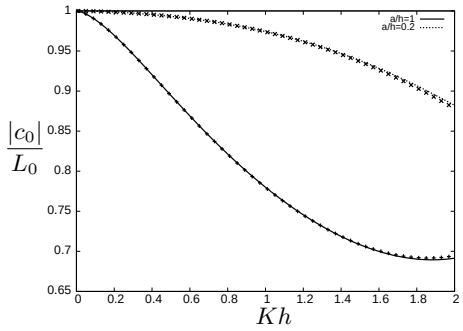

Figure 7. The damping effect $|c_0|/L_0$ for a wavemaker next to a fixed screen of porosity $p = 0.25$, for $\frac{\epsilon}{h} = 0.025$ and two bay widths, $\frac{a}{h} = 1$ and 0.2.

Evaluating the components of the line integral along the boundary S, we see that the integrand along $y = 0$ and $y = h$ is zero and only contributions along $x = -a$, $x = \pm 0$ and as $x \to \infty$ remain. At the wavemaker we have that $\phi_x = 1$, whilst as $x \to \infty$ the evanescent terms in the potential decay to zero and we are only left with the propagating mode. Thus application of (3.20) to $x > 0$ gives,

$$0 = -\int_{x=0^+} \Im\left\{\phi\bar{\phi}_x\right\} \mathrm{d}y - \frac{|c_0|^2 h}{k}, \tag{3.21}$$

and in $-a < x < 0$ gives

$$0 = \int_{x=0^-} \Im\left\{\phi\bar{\phi}_x\right\} \mathrm{d}y - \int_{x=-a} \Im\left\{\phi\right\} \mathrm{d}y. \tag{3.22}$$

We note that the latter integral is just proportional to the imaginary part of the pressure force on the wavemaker and so

$$\int_{x=-a} \Im\left\{\phi\right\} \mathrm{d}y = -\frac{m}{\rho}\nu_w \tag{3.23}$$

where ν_w is the damping on the wavemaker and $m = 2\rho a h$ the mass of water contained between the wavemaker and the screen. Thus summing the contributions from each region we have,

$$\int_{x=0} \Im\left\{[\phi]^+_-\bar{\phi}_x\right\} \mathrm{d}y = -\frac{|c_0|^2 h}{k} + \frac{m}{\rho}\nu_w, \tag{3.24}$$

where we evaluate the damping coefficient at the wavemaker to be,

$$\frac{m}{\rho}\nu_w = \left(2b_0 \mathrm{e}^{\mathrm{i}ka} - L_0\right)\frac{L_0}{\mathrm{i}k} + \sum_{n=1}\left(2b_n \mathrm{e}^{-k_n a} - L_n\right)\frac{L_n}{-k_n}. \tag{3.25}$$

The rate of work done to displace the wavemaker, which can be expressed as

$$W_{in} = \tfrac{1}{2}\Re\left\{\mathrm{i}\omega\rho\int_0^h \phi\bar{\phi}_x \mathrm{d}y\right\} = -\tfrac{1}{2}\omega\rho\int_0^h \Im\{\phi\}\ \mathrm{d}y = \tfrac{1}{2}m\omega\nu_w, \quad (3.26)$$

is then used to nondimensionlise the power loss at the screen and thus we write,

$$P_{loss} = \frac{W_{out}}{W_{in}} = 1 - \frac{|c_0|^2}{ka\nu_w}. \quad (3.27)$$

We also determine the far-field radiated wave amplitude $\hat{A}_\infty$. The far-field radiated wave coefficient is c_0 and the dimensionless far-field waves, from (3.6) in (3.13), are described by

$$\frac{\eta(x)}{h} = \hat{A}_\infty \mathrm{e}^{\mathrm{i}kx}, \qquad x \to \infty \quad (3.28)$$

where

$$\hat{A}_\infty = N_0^{-1/2}\hat{\epsilon}\sinh khc_0. \quad (3.29)$$

Thus, we can use the solution to the non-linear problem (3.18) to compare far-field radiated wave amplitudes from the linearised solution (3.12) when blockage effects are switched off ($\mathbb{C} = 0$ or $\gamma = \mathrm{i}\mathbb{K}_L$).

These comparisons are shown in figure 6 and 7. When no screen is present, the solution is (3.29) with L_0 replacing c_0. Thus, we consider the damping effect c_0/L_0. Figure 6(a) and (b) show results for a screen of porosity $p = 0.25$ and $p = 0.75$ respectively. The bay width is taken to be $\frac{a}{h} = 5$ and oscillation amplitudes are varied. The agreement between the fully non-linear and equivalent linear results is excellent. In figure 7 we narrow the bay width, an arrangement where we might expect slightly less good agreement as we are using a drag coefficient determined from an unbounded problem, however results still fit across a full range of kh.

Once could argue that solving (3.18) directly is an easier route to determining an equivalent linear drag condition, rather than iterating towards a solution which itself calculates a linear drag coefficient from a different problem. However, once a blockage coefficient is included, the value of a_0, the wave amplitude incident upon the screen is altered and the iterative scheme takes this into account, whilst the calculation of (3.18) has isolated the drag from the inertia. The argument is therefore made in favour of the iterative scheme.

In figure 8 we combine the both the drag and inertia coefficients, as in (2.49). For a screen of given porosity, as the number of gaps in the screen are increased and it tends to a porous screen, $kd \to 0$.

Considering figure 2 and (2.31), in this limit $\mathbb{C} \to 0$ and the inertial effects are diminished. In panel (a) of figure 8 we show results for a screen with 5 gaps and panel (b) 50 gaps and compare with the results obtained when we isolated the effects of drag. As expected for a screen with 50 gaps there is less influence of the inertial effects. Figure 8 show results for a screen of porosity $p = 0.25$, for screens of higher porosity, the inertial coefficient $\mathbb{C}$ will be smaller for fixed wave number k as in (2.29).

Points at which $c_0/L_0 = 1$ in figure 6 relate to sloshing frequencies of the bay region between the wavemaker and the screen. Notice that in figure 8 (a), for a screen with 5 gaps there are some frequencies at which $c_0/L_0 > 1$ when we include the inertial effects of the screen. This is more pronounced for smaller forcing amplitudes. This is an unexpected result which suggests that the wave amplitudes at infinity in the presence of a screen are larger in those frequency intervals than if the screen were not present. Note that the screen is still taking power out of the system, as in figure 8 (e) and (f), though presumably the work done in moving the wavemaker is much greater than in the absence of the screen.

3.2. Waves incident in a screen in front of a wall

In the previous demonstration, waves were incident on the screen from only one direction ($x < 0$) due to the wavemaker. Here, we send in a wave from $x = -\infty$ of prescribed dimensionless amplitude $\hat{A}$ to a fixed screen at $x = 0$, but by placing a vertical perfectly reflecting wall at $x = a$ allow travelling waves to approach the screen from both directions.

We set up eigenfunction expansions in $x < 0$ as

$$\phi = (\mathrm{e}^{\mathrm{i}kx} + R\mathrm{e}^{-\mathrm{i}kx})\psi_0(y) - \sum_{n=1}^{\infty} a_n \mathrm{e}^{k_n x}\psi_n(y) \tag{3.30}$$

and in and $0 < x < a$

$$\phi = (b_0\mathrm{e}^{-\mathrm{i}k(x-a)} + c_0\mathrm{e}^{\mathrm{i}kx})\psi_0(y) + \sum_{n=1}^{\infty}\left(b_n\mathrm{e}^{k_n(x-a)} + c_n\mathrm{e}^{-k_n x}\right)\psi_n(y), \tag{3.31}$$

which satisfies Laplace's equation throughout the fluid and the boundary conditions on $y = 0$ and $y = h$ given by (2.2). We also need to impose

$$\phi_x = 0 \quad \text{on} \quad x = a, \tag{3.32}$$

a no flow condition on the wall, which gives us that

$$b_n = c_n\mathrm{e}^{-k_n a}, \qquad n \geq 0. \tag{3.33}$$

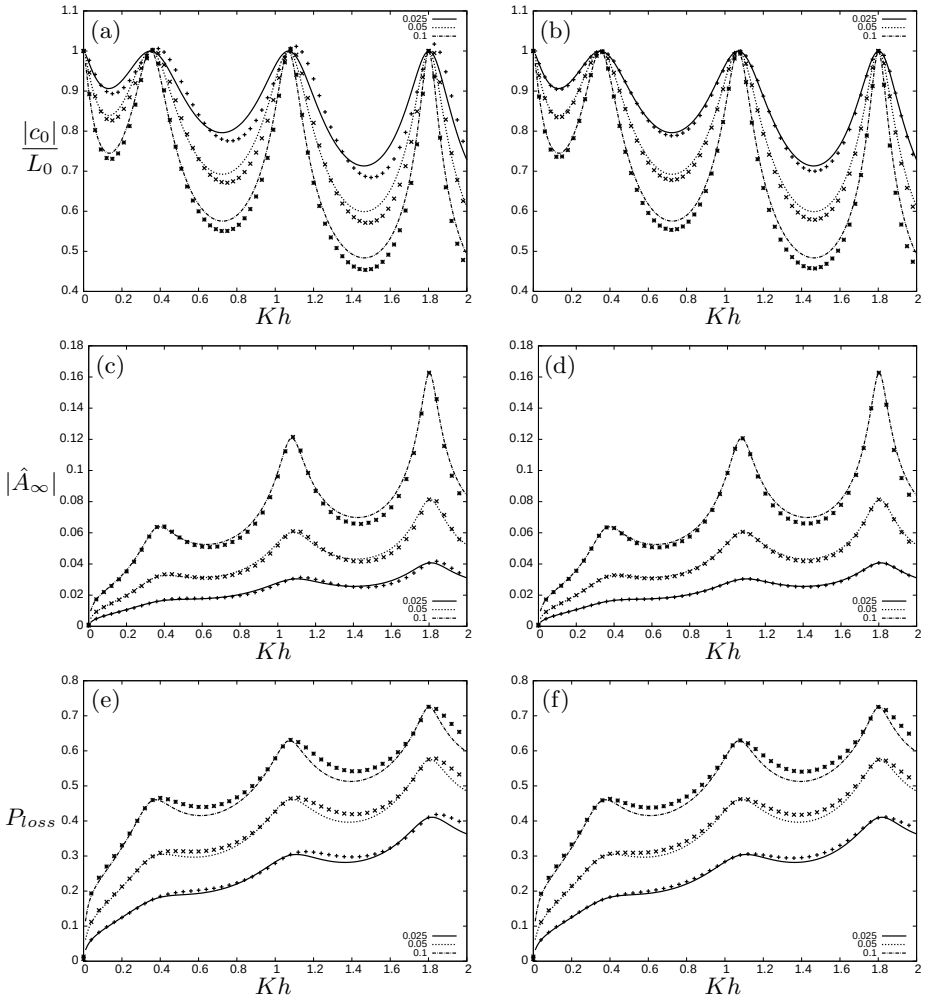

Figure 8. $|c_0|/L_0$, $|\hat{A}_\infty|$ and P_{loss} for a wavemaker next to a fixed screen of porosity $p = 0.25$, with $\frac{a}{h} = 5$ for varying oscillation amplitudes $\frac{\epsilon}{h} = 0.025, 0.05$ and 0.1, including inertial effects. In panel (a), (c) and (e): For a screen with 5 gaps. In panel (b), (d) and (f): For a screen with 50 gaps. Lines show results when the effects of drag are isolated and the crosses the results when the effects of both drag and inertia are included.

Additionally, continuity of velocity at the screen, (2.3) gives the relation

$$c_n = \frac{a_n}{1 - \mathrm{e}^{-2k_n a}}, \qquad n \geq 0, \tag{3.34}$$

where $a_0 = 1 - R$. Finally, it remains to apply our screen averaged condition (3.10). Matching the $n = 0$ mode, it follows that

$$1 - \frac{a_0}{1 - \mathrm{e}^{2\mathrm{i}ka}} = \mu_0 a_0, \tag{3.35}$$

such that,

$$a_0 = \frac{1 - \mathrm{e}^{2\mathrm{i}ka}}{1 + \mu_0(1 - \mathrm{e}^{2\mathrm{i}ka})}, \tag{3.36}$$

where we recall that $R = 1 - a_0$ is the reflection coefficient, and $\mu_0 = \mathrm{i}\gamma/2$ with $\gamma = \mathbb{C} + \mathrm{i}\mathbb{K}_L$. Thus, if $\mathbb{K}_L$ is known - after being found using the same iterative procedure as in the previous section - then R can be determined.

Notice that if $\mathbb{K}_L \to \infty$, and the screen becomes solid then $a_0 \to 0$ and $R = 1$ as expected. Additionally if $\mathbb{K}_L \to 0$, as if there were no barrier in the way, then $R = \mathrm{e}^{2\mathrm{i}ka}$. Here the dimensionless power loss at the screen is simply $P_{loss} = 1 - |R|^2$, therefore in this section we only consider the reflection coefficient $|R|$.

As opposed to making comparisons with results obtained through solving the fully non-linear system and considering the effects of including or neglecting inertia, as in the previous section, here we can compare our theoretical results with scaled experiments conducted by Bennett *et al.* (1992) to determine the reflection coefficient R for a porous screen with an impermeable backing wall.

As an additional measure of the accuracy of our results, it is useful to note that the screen at $x = 0$ were solid then resonant behaviour would be expected near the sloshing frequencies of the region contained by the wall and the screen. These frequencies are given by $Kh = n\pi h/a \tanh(n\pi h/a)$.

In figure 9 we compare the results of our equivalent linearised problem, including both drag and inertia, with the experimental results of Bennett *et al.* (1992) and use this as a measure in determining the accuracy of our model approximation. The reflection coefficient is plotted against the frequency f (in Hz.), where $f = \omega/(2\pi)$. Our results show much similarity to the theoretical solutions presented by Bennett *et al.* (1992), with good correspondence between the location of peaks in the reflection coefficient and frequencies at which standing waves would be expected if the screen were impermeable. Although there is still some disparity when the screen is of very low porosity in figure 9(f), and when the screen is closer to the wall as in figure 9(a), our model shows better agreement with experimental results here than in figure 5.

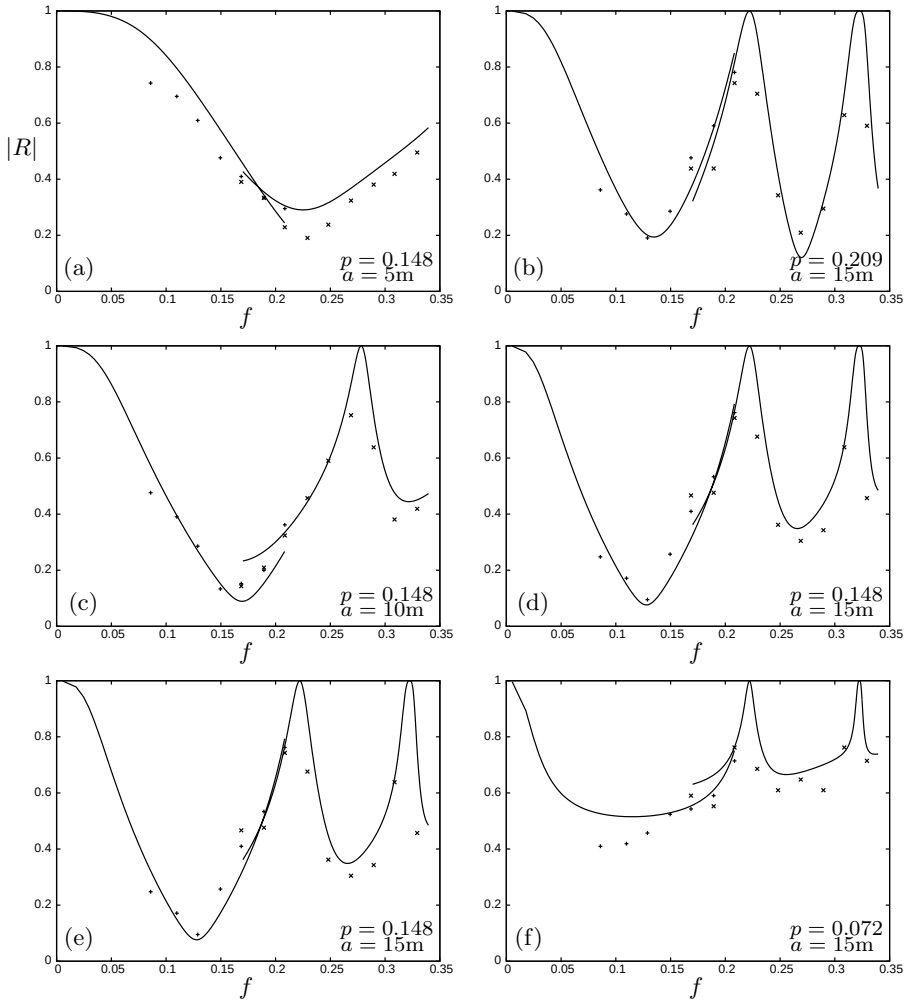

Figure 9. $|R|$ against frequency in Hz. for a wave incident to a screen of varying porosity in front of a wall compared with experimental data from Bennett *et al.* (1992). The two sets of results seen in each plot correspond to the experimental tests that were performed for two wave spectra for incident waves of amplitude $\hat{A} = 0.0372$ (+) and $\hat{A} = 0.0581$ (×) covering frequencies relating to wave periods of $4.5 - 14\,\mathrm{s}$ and $2.9 - 6.2\,\mathrm{s}$ respectively.

3.3. Forced sloshing of waves in a rectangular tank

A study not reported in this paper, on a wavemaker next to a moving slatted screen, shows very good agreement between fully nonlinear and linear calculations even though the screen condition has been modified to account for the relative velocity between the fluid and the moving

screen. On this basis, we feel confident that this procedure will work effectively in this tank sloshing problem where both walls and screen are moving simultaneously.

The configuration is now of a rectangular tank filled with fluid to a depth h with vertical sides at $x = \pm a$ and a centrally-placed screen at $x = 0$, all forced to oscillate in tandem with dimensionless amplitude $\hat{\epsilon}$ and frequency ω. Thus, the tank includes features from both previous examples. The aim is to determine the solution using linearised screen-averaged conditions derived from the canonical problems considered in §2. In particular we focus on the components of the complex horizontal force induced by the fluid motion on the tank, the so-called added mass and damping coefficients.

The governing equations for this system are again given by (2.1)–(2.4), where now $V(y,t) \equiv \Phi_x(0,y,t) - \omega\epsilon\cos\omega t$ is the relative horizontal velocity of the fluid to that of the screen.

As before, we decompose the potential as in (3.2). It is clear that the oscillations will be antisymmetric, such that $\phi(x,y) = -\phi(-x,y)$, then we only need consider the boundary conditions on the half tank in $x < 0$. On the vertical wall of the tank, the horizontal velocity of the fluid, when linearised is equivalent to

$$\phi_x = 1, \qquad \text{on } x = -a, \quad 0 < y < h. \tag{3.37}$$

At the screen, the condition for continuity of velocity (2.8) still holds, however the dynamic linearised screen-averaged condition with antisymmetry is now written as

$$-2\phi(0^-,y) = \frac{\gamma}{k}\left(\phi_x(0^-,y) - 1\right), \qquad 0 < y < h. \tag{3.38}$$

We construct eigenfunction expansions in the region $x < 0$ of the form,

$$\begin{aligned}\phi(x,y) =& \frac{1}{\mathrm{i}k}\left(a_0\mathrm{e}^{\mathrm{i}k(x+a)} - b_0\mathrm{e}^{-\mathrm{i}kx}\right)\psi_0(y) \\ &- \sum_{n=1}^{\infty}\frac{1}{k_n}\left(a_n\mathrm{e}^{-k_n(x+a)} - b_n\mathrm{e}^{k_nx}\right)\psi_n(y).\end{aligned} \tag{3.39}$$

Applying (3.37) to (3.39) we obtain a relation between coefficients,

$$a_n = -b_n\mathrm{e}^{-k_na} + L_n \qquad \text{for } n \geq 0. \tag{3.40}$$

To simplify the algebra, we introduce coefficients d_n for $n = 0, 1, 2\ldots$ such that

$$\phi_x(0,y) - 1 = d_0\psi_0(y) + \sum_{n=1}^{\infty} d_n\psi_n(y), \tag{3.41}$$

where

$$d_n = L_n\left(\mathrm{e}^{-k_n a}-1\right)+b_n\left(1-\mathrm{e}^{-2k_n a}\right) \qquad \text{for } n\geq 0. \tag{3.42}$$

Thus, applying (3.38) to (3.39) using the relations (3.40) and (3.42), multiplying by $\psi_m(y)$ for $m \geq 0$ and integrating over the depth $[0,h]$ we obtain,

$$\frac{1}{-k_n}\left(\frac{L_n(\mathrm{e}^{-k_n a}-1)^2+d_n(1+\mathrm{e}^{-2k_n a})}{1-\mathrm{e}^{-2k_n a}}\right)=\frac{\gamma}{2k}d_n. \tag{3.43}$$

Rearranging, we have that

$$d_n\left(\mu_n(1-\mathrm{e}^{-2k_n a})+(1+\mathrm{e}^{-2k_n a})\right)=-L_n(\mathrm{e}^{-k_n a}-1)^2, \tag{3.44}$$

for $n \geq 0$, where $\mu_n = \gamma k_n/(2k)$. Once the d_n's are known we find the added mass and damping and compare with the fully non-linear counterpart for our sloshing problem to assess the accuracy of our equivalent linearised results. The non-linear condition at the screen, isolating the drag effects assuming that $L = 0$, is given by

$$[\phi]_{x=0^-}^{x=0^+}=\mathrm{i}\frac{\mathbb{K}_{NL}}{k^2}\left(\phi_x(0,y)-1\right)\left|\phi_x(0,y)-1\right|. \tag{3.45}$$

Applying this we obtain a non-linear system of equations,

$$-2\frac{d_m\left(\mathrm{e}^{-2k_m a}+1\right)+L_m\left(\mathrm{e}^{-k_m a}-1\right)^2}{k_m h(1-\mathrm{e}^{-2k_m a})}= \mathrm{i}\mathbb{K}_{NL}\sum_{n=0}^{\infty}\frac{d_n}{h}\int_0^h\left|\sum_{r=0}^{\infty}d_r\psi_r(y)\right|\psi_n(y)\psi_m(y)\mathrm{d}y. \tag{3.46}$$

We implement the same numerical procedure as before, introducing a scaling factor to the right-hand side which increases from zero, where now the solution $d_m = -L_m\left(\mathrm{e}^{-k_m a}-1\right)^2/\left(\mathrm{e}^{-2k_m a}+1\right)$ is explicit, to unity.

Once the d_m's have been found, we can calculate the hydrodynamic forces exerted on the tank by the sloshing motion of the fluid, using the integrated pressure over the tank walls and screen, to be

$$F=-2\mathrm{i}\omega\rho\int_0^h\left(\phi(0^-,y)-\phi(-a,y)\right)\mathrm{d}y, \tag{3.47}$$

where the factor of two comes from the fact that $\phi(x,y)$ is antisymmetric. Decomposing F into its real and imaginary parts and nondimensionalising with respect to the mass of the water in the tank $m = 2\rho a h$ gives,

$$F=-\mathrm{i}\omega m\left(\mu+\mathrm{i}\nu\right), \tag{3.48}$$

where μ is the non dimensional added mass and ν the damping. The net horizontal force can be explicitly integrated to be

$$F = -\,\mathrm{i}\omega m \left(\frac{L_0}{\mathrm{i}ka} \frac{(\mathrm{e}^{\mathrm{i}ka}-1)^2}{(\mathrm{e}^{2\mathrm{i}ka}-1)} (d_0 + 2L_0) + \sum_{n=1}^{\infty} \frac{L_n}{-k_n a} \frac{(\mathrm{e}^{-k_n a}-1)^2}{\mathrm{e}^{-2k_n a}-1} (d_n + 2L_n) \right). \quad (3.49)$$

Figures 10 and 11 plot the added mass and damping coefficients μ and ν for tanks of aspect ratio $a/h = 4$ and $a/h = 2$ respectively. We notice that in the limit of the forcing frequency going to zero $\mu \to 1$, that is to say that the added mass tends to the mass of water in the tank, and $\nu \to 0$ which is as to be expected. We look to compare the effect of varying a/h, ϵ/h and the porosity of the screen. As before we consider the effect of linearised drag (i. e. ignore inertia) on the screen and compare the approximate with the full nonlinear drag calculations. As expected better agreement with the fully non-linear results is seen for wider tanks and thus, screens of higher porosity also. Consider panels (a), (b) and (c) of figures 10 and 11 as ϵ/h is increased from 0.0125 to 0.05, greater deviation is seen from the solution to the non-linear problem. Further numerical investigations with screens of mid porosity, give good agreement across a range of forcing amplitudes.

In figure 12 we look at the absolute value of the equivalent linear drag coefficient $|\mathbb{K}_L|$ that the iterative method outlined in §3.1 outputs. We note that for small kd there is an approximate linear relationship between $|\mathbb{K}_L|$ and ϵ/h, which will be useful when applying this approach to more complicated problems involving multiple screens in tanks for example.

Finally we include inertia in our screen boundary condition. Inertial effects, shown in figure 13, despite altering the results to a lesser degree than in previous settings considered, are seen to be more pronounced for screens of lower porosity as predicted by Tuck's (1975) and Mei's (1983) long wavelength result (2.29).

4. Conclusions

In this paper an investigation has been conducted into the effect of a thin slatted barrier upon the propagation of waves. A canonical problem of waves from infinity incident on a single slatted barrier, incorporating a detailed model of the non-linear flow conditions across the screen, has been used to develop equivalent linear screen-averaged conditions. These linear conditions have been applied across screens in a series of

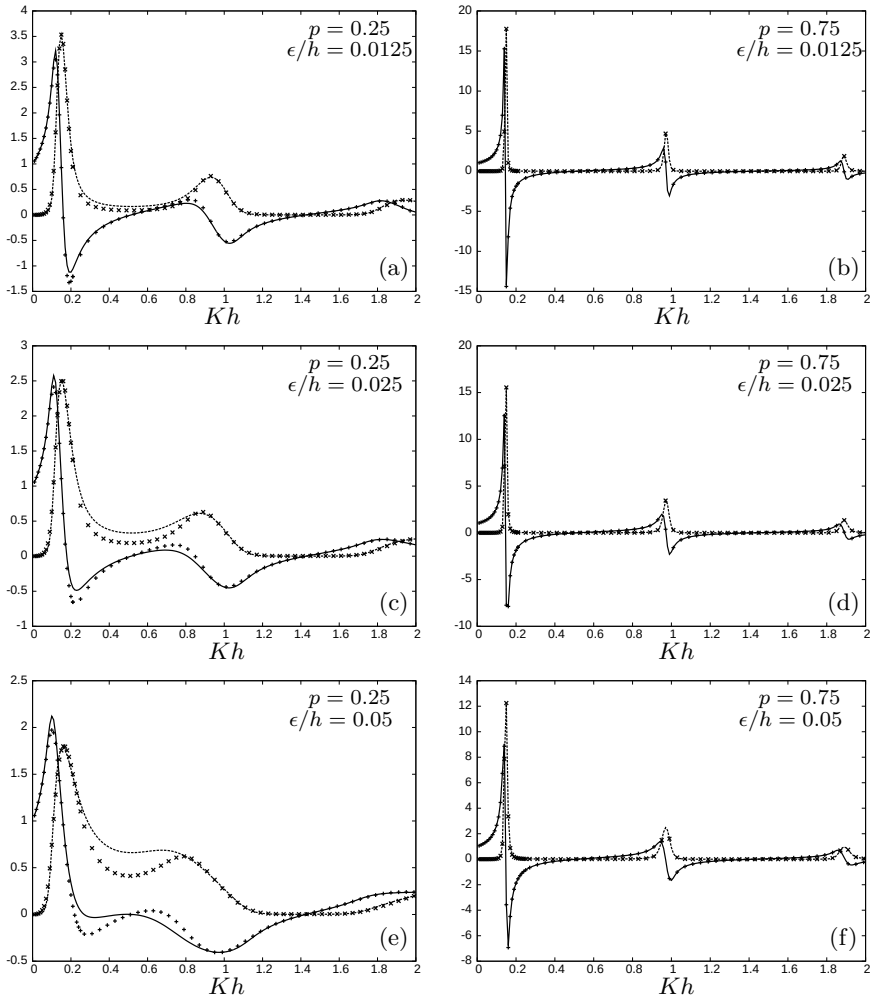

Figure 10. Added mass and damping coefficients μ and ν, shown by a solid and dashed line respectively, for a forced tank with a centrally placed screen. Tank aspect ratio $\frac{a}{h} = 4$ for each panel. Lines show the fully non-linear results and the crosses the equivalent linear results.

model problems involving slatted barriers in other settings. The aim of this paper has been to show that these equivalent linear conditions derived from the canonical problem provide a good approximation to the exact solutions in a variety of problems. This has been demonstrated by comparing results with a direct non-linear calculation arising from application of the quadratic drag law directly to each of these settings.

The work of Mei *et al.* (1983) and Bennett *et al.* (1992) form the basis of the approach for the canonical problem of waves incident on

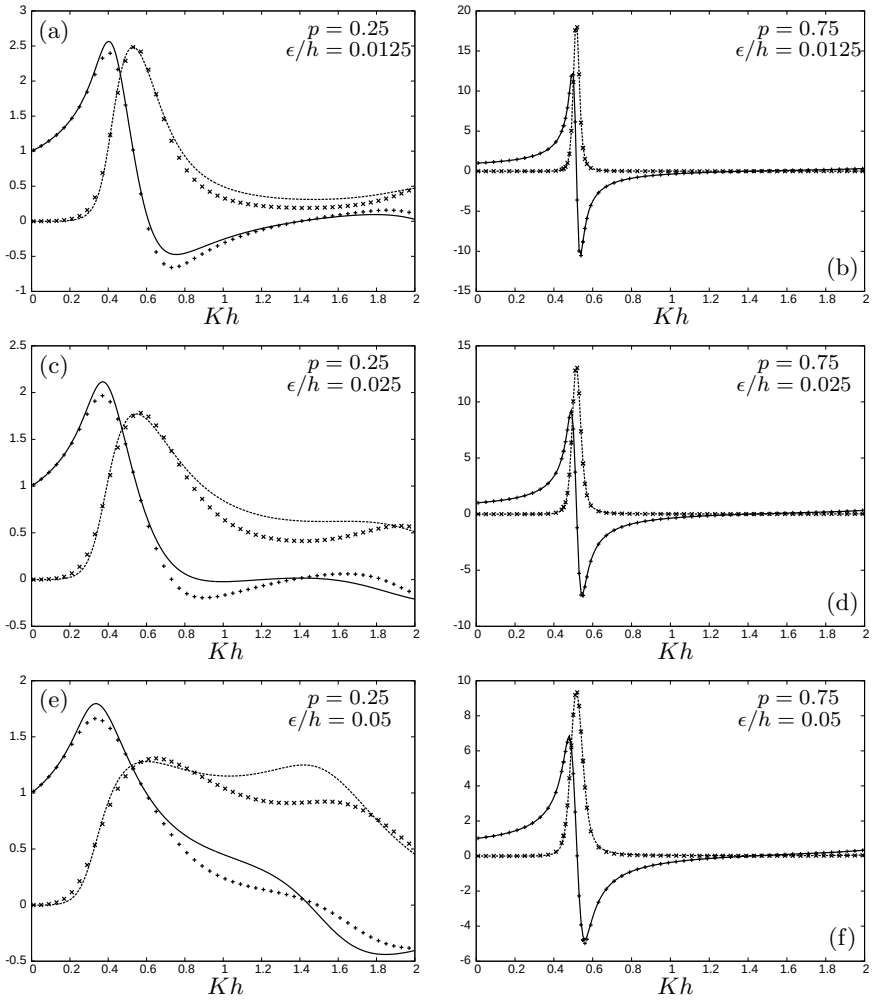

Figure 11. Added mass and damping coefficients μ and ν, shown by a solid and dashed line respectively, for a forced tank with a centrally placed screen. Tank aspect ratio $\frac{a}{h} = 2$ in each panel. Lines show the fully non-linear results and the crosses the equivalent linear results.

a single screen. The effects of drag and inertia are isolated from one another and treated separately. An equivalent screen averaged inertia coefficient is found from a considering the precise slat/gap structure of the screen and is shown to agree with the asymptotic result of Tuck (1975) in the long wavelength limit. An equivalent linear drag coefficient has been derived from consideration of the solution of the non-linear problem in which a quadratic turbulent drag law is imposed across the screen.

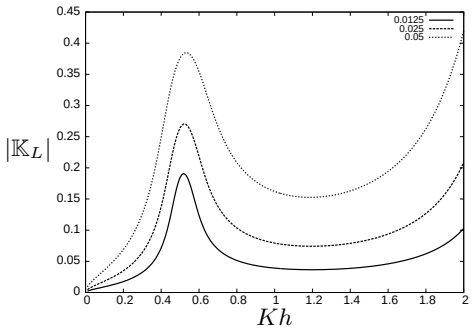

Figure 12. The absolute value of the equivalent linear drag coefficient $|\mathbb{K}_L|$ for a single centrally placed screen of porosity $p = 0.5$ in a forced tank with aspect ratio $\frac{a}{h} = 5$, results for $\frac{\epsilon}{h} = 0.0125, 0.025$ and 0.05.

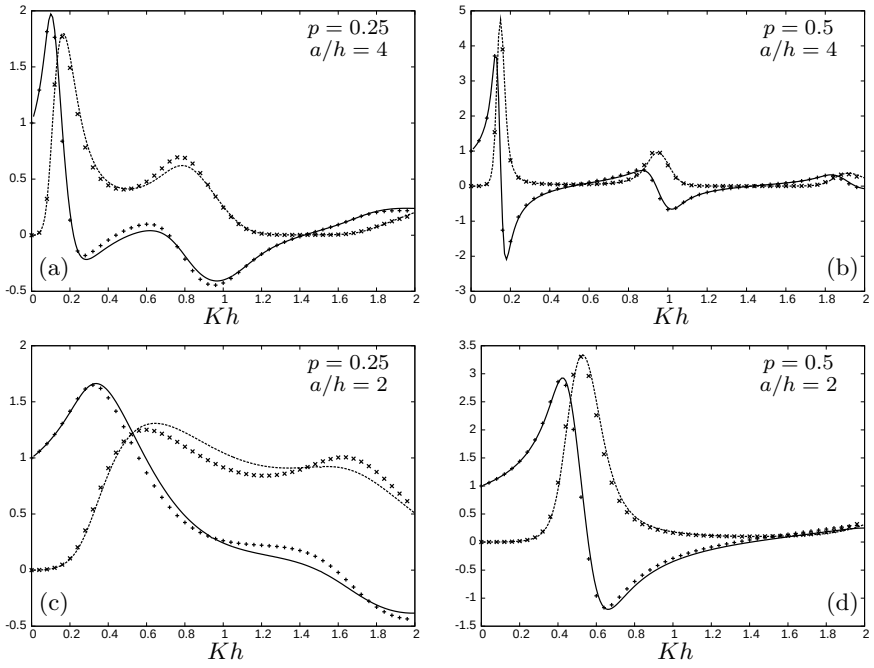

Figure 13. Added mass and damping coefficients μ and ν, shown by a solid and dashed line respectively, for a forced tank with a centrally placed screen with five gaps. In all panels $\frac{\epsilon}{h} = 0.05$. Lines show the equivalent linear results with drag effects only, crosses with both drag and inertial effects included.

The results of the linearised approximation are shown to give good qualitative agreement with those from an exact non-linear solution of each of the model problems. Comparisons of the calculated reflection coefficient from waves incident on a vertical slatted screen in front of a backing wall with the experimental results of Bennett *et al.* (1992) show excellent agreement.

We find that for a screen of given porosity and for fixed wavenumber, k, as the number of gaps in the screen is increased and the barrier tends to a thin porous screen the inertial effects are diminished. Similarly for a screen with a given number of gaps, inertial effects are seen to decrease with an increase in screen porosity, for fixed wavenumber k.

It is envisaged that this approach could be extended to more complicated problems, such as problems involving more than one screen or with application to TLDs, where a direct nonlinear calculation becomes algebraically difficult. Numerical evidence suggests that for low frequency wave motion the equivalent linear drag coefficient is approximately proportional to the forcing amplitude, it may be possible to take advantage of this fact when looking at low frequency oscillations of rectangular tanks with multiple screens, for example.

References

Baines, W D & Peterson, E G 1951. An investigation of flow through screens. Trans. ASME 73, 467–479.

Bennett, G S, McIver, P and Smallman, J V 1992. A mathematical model of a slotted wavescreen breakwater. Coastal Engineering. 18, 231–249.

Dalrymple, R A, Losada, M A and Martin, P A 1991. Reflection and transmission from porous structures under oblique wave attack. Journal of Fluid Mechanics. 224, 624–644.

Evans, D V 1976. A theory for wave-power absorption by oscillating bodies. Journal of Fluid Mechanics. 77(1), 1–25.

Evans, D V 1990. The use of porous screens as wave dampers in narrow wave tanks. Journal of Engineering Mathematics. 24(3), 203–212.

Faltinsen, O M, Firoozkoohi, R and Timokha, A N 2010. Analytical modeling of liquid sloshing in a two-dimensional rectangular tank with a slat screen. Journal of Engineering Mathematics. 70, 93–109.

Faltinsen, O M & Timokha, A N 2011. Natural sloshing frequencies and modes in a rectangular tank with a slat-type screen. Journal of Sound and Vibration. 330, 1490–1503.

Faltinsen, O M, Firoozkoohi, R and Timokha, A N 2011. Steady-state liquid sloshing in a rectangular tank with a slat-type screen in the middle: Quasilinear modal analysis and experiments. Physics of Fluids. 23(4), Art. No. 042101.

Gradshteyn, I S & Ryzhik, I M 1980. Table of Integrals, Series and Products, Fourth Edition. New York: Academic Press.

Isaacson, M, Premasiri, S and Yang, G 1998. Wave interactions with vertical slotted barrier Journal of waterway, port, coastal, and ocean engineering. 124(3), 118–126.

Kondo, H & Toma, S 1972. Reflection and transmission for a porous structure Proc. 13th Coastal Eng. Conf. 1847–1866.

Madsen, O S 1974. Wave transmission through porous structures Journal of the Waterways, Harbors and Coastal Engineering Division. 100(3), 169–188.

McIver, P 1999. Water-wave diffraction by thin porous breakwater Journal of waterway, port, coastal, and ocean engineering. 125, 66–70.

McIver, P 2005. Diffraction of water waves by a segmented permeable breakwater Journal of waterway, port, coastal, and ocean engineering. 131, 69–76.

Mei, C C 1976. Power extraction from water waves. Journal of Ship Research. 20, 63–66.

Mei, C C 1983. The Applied Dynamics of Ocean Surface Waves. World Scientific.

Newman, J N 1976. The interaction of stationary vessels with regular waves. Proc. 11th Symposium on Naval Hydrodynamics. 491–501.

Porter, R & Evans, D V 1995. Complementary approximations to wave scattering by vertical barriers. Journal of Fluid Mechanics. 294, 155–180.

Sollitt & Cross, R H 1972. Wave transmission through permeable breakwaters. Proc. 13th Coastal Eng. Conf. 1827–1846.

Sulisz, W 1985. Wave reflection and transmission at permeable breakwaters of arbitrary cross-section Journal of Coastal engineering. 9(4), 371–386.

Tait, M J, El Damatty, A A, Isyumov, N and Siddique, M R 2005. Numerical flow models to simulate tuned liquid dampers (TLD) with slat screens. Journal of Fluids and Structures. 20, 1007–1023.

Tait, M J 2008. Modelling and preliminary design of a structure-TLD system. Engineering Structures. 30(10), 2644–2655.

Tuck, E O 1975. Matching problems involving flow through small holes. Advances in Applied Mechanics. 15, 89–158.

Wu, J, Wan, Z, and Fang, Y 1998. Wave reflection by a vertical wall with a horizontal submerged porous plate. Ocean engineering. 25(9), 767–779.

Yu, X 1995. Diffraction of water waves by porous breakwaters. Journal of waterway, port, coastal, and ocean engineering. 121, 275–282.